

Article

# Fundamental Oscillation Modes in Neutron Stars with Hyperons and Delta Baryons

O. P. Jyothilakshmi <sup>1</sup>, P. E. Sravan Krishnan <sup>2</sup>, V. Sreekanth <sup>1,\*</sup>, Harsh Chandrakar <sup>3</sup> and Tarun Kumar Jha <sup>3</sup>

<sup>1</sup> Department of Physics, Amrita School of Physical Sciences, Amrita Vishwa Vidyapeetham, Coimbatore 641112, India; op\_jyothilakshmi@cb.students.amrita.edu

<sup>2</sup> Argelander-Institut für Astronomie, Universität Bonn, Auf dem Hügel 71, 53121 Bonn, Germany; s27skris@uni-bonn.de

<sup>3</sup> Department of Physics, BITS PILANI K K Birla Goa Campus, Goa 403726, India; p20220023@goa.bits-pilani.ac.in (H.C.); tkjha@goa.bits-pilani.ac.in (T.K.J.)

\* Correspondence: v\_sreekanth@cb.amrita.edu

**Abstract:** For a new parameterization of the modified effective chiral model, developed primarily to regulate the density content of the symmetry energy and its higher order terms, equations of state (EoSs) for hyperon-rich matter ( $H$ ) and delta baryon matter ( $\Delta$ ) were obtained. The models were used to investigate the emission of gravitational waves (GWs) through  $f$ -mode oscillations in the corresponding neutron stars. We obtained the stellar structure,  $f$ -mode frequency and tidal deformability  $\Lambda$  for our models. We report that the  $\Delta$  EoS is stiffer compared to the  $H$  EoS. We also analyzed the velocity of sound in these media. The corresponding mass–radius relationships were obtained and compared with various observations. We studied the dependence of  $f$ -mode frequencies on the stellar mass, redshift and tidal deformability. We employed the well known Cowling approximation to obtain the  $f$ -mode frequencies for  $l = 2, 3$  and  $4$  modes of oscillation. We found that the  $f$ -mode frequencies of the  $H$  and  $\Delta$  EoSs were almost the same in the lower mass region, while we observed a substantial difference between them in the high-mass region. We also obtained an empirical relation for the EoSs considered. The various attributes obtained for our models showed close agreement with various observational constraints from pulsars and GW events.

**Keywords:** Neutron stars, Oscillations, Equations of state



Academic Editor: Firstname Lastname

Received: 4 October 2024

Revised: 29 January 2025

Accepted: 30 January 2025

Published:

**Citation:** Jyothilakshmi, O.P.; Krishnan, P.E.S.; Sreekanth, V.; Chandrakar, H.; Jha, T.K. Fundamental Oscillation Modes in Neutron Stars with Hyperons and Delta Baryons. *Symmetry* **2025**, *1*, 0. <https://doi.org/>

**Copyright:** © 2025 by the authors. Licensee MDPI, Basel, Switzerland. This article is an open access article distributed under the terms and conditions of the Creative Commons Attribution (CC BY) license (<https://creativecommons.org/licenses/by/4.0/>).

## 1. Introduction

The detection of gravitational waves (GWs) from binary neutron star mergers [1–3] has opened up a new way to constrain the equation of state (EoS) of dense matter found inside neutron stars. This is in addition to the basic constraint of meeting the maximal mass criteria set by the most massive of the observed pulsars, examples of which are PSR J0348–0432 [4], PSR J1614–2230 [5] and PSR J0740+6620 [6]. Neutron stars (NSs) could experience a significant loss in angular momentum through the emission of GWs, which could potentially be detected by the upcoming Einstein Telescope or even by the Advanced LIGO/VIRGO.

External perturbations can send NSs into oscillation in various quasi-normal modes, and these modes emit gravitational waves. Well-known NS oscillation modes include the fundamental ( $f$ ) modes, pressure ( $p$ ) modes, rotational ( $r$ ) modes and gravitational ( $g$ ) modes. Gravitational radiation can cause both the  $f$ - and  $r$ -modes to become unstable through the Chandrasekhar–Friedman–Schutz mechanism [7,8], and this instability can be

arXiv:2502.04264v1 [astro-ph.HE] 6 Feb 2025

damped by dissipative effects such as the shear and bulk viscosities [9–14]. However, it was found that unlike with  $r$ -modes, the damping of  $f$ -modes leaves only a small region of instability [11] in the plot between the angular velocity  $\Omega$  and core temperature  $T$ . An unstable  $f$ -mode could have enough strength to be detected by gravitational wave observatories [15]. If detected, these gravitational waves could provide a better understanding of the nature of the matter within NSs.

The study of these oscillation modes requires solving the perturbed fluid equations in general relativity. The first integrated numerical solution for  $f$ -modes was obtained by the authors of Ref. [16] for various EoSs. The relativistic Cowling approximation [17], obtained by neglecting the metric perturbations while considering the fluid oscillations, is widely used to study  $f$ -mode oscillations in compact stars. This approximation was found to differ from the general relativistic treatment by less than 20% [18]. It was used to study non-radial oscillations in compact stars in Refs. [19–21]. More recently, the Cowling approximation was used to estimate the  $f$ -mode frequencies for various other stellar configurations, such as bosonic dark matter [22], hyperon [23], hybrid [24], dark matter-admixed hyperon [25] and dark energy [26] stars. An important constraint on the EoS is given by the analysis of the gravitational wave signal emitted during a binary inspiral, which is characterized by the tidal deformability ( $\Lambda$ ). It measures the quadrupole deformation of the star due to the tidal field of a companion star. This is over and above the constraints already provided by the electromagnetic observations of neutron stars, which include their masses, radii, gravitational redshift and spin among others (see Ref. [27]). The GW170817 measurements provided limits on the radius and tidal deformability of a canonical NS ( $1.4M_{\odot}$ ) in the range of  $R_{1.4} = 12\text{--}13.5$  km and  $\Lambda_{1.4} = 190^{+390}_{-120}$ , respectively [2]. Additionally, a range for the  $f$ -mode frequency was obtained as 1.67–2.18 kHz [28]. Future measurements from binary NS mergers may impose more strict limits on  $f$ -mode frequencies.

The present model was treated very similarly to the well-known relativistic mean field approach to account for many baryon systems. Introduced by Gell-Mann and Levy [29], it was subsequently applied to nuclear matter studies [30]. After a series of modifications [30–36], the model was used to describe finite nuclear properties [37–39]. Further, the inclusion of the dynamically generated mass of the vector meson in the model [40,41] resulted in an unrealistically high nuclear incompressibility ( $K$ ) value, which was reduced to an acceptable range by introducing higher order terms of the scalar meson field and then applied to nuclear matter studies [42]. Lately, mesonic cross-couplings have been incorporated [43] to regulate the density dependence of the symmetry energy parameters, and this was applied to study magnetized neutron stars [44]. It is to be noted that higher order interactions in the chiral fields are desirable as they are known to mimic three-body forces, which may play a vital role in dense matter studies.

With the ever-growing observations of massive stars, the role of exotic matter such as quarks, hyperons, etc., in compact stars has become interesting and important, particularly since very little is known about nucleon–hyperon, hyperon–hyperon or delta’s interaction in matter. The observation of high-mass pulsars severely constrains the EoS and therefore the particle interactions, particularly when one considers exotics like hyperons or quarks in their inner shells. Their presence is known to have a softening effect on the EoS on one hand, while on the other hand we require a stiffer EoS in order to achieve a massive neutron star configuration. There are several prescriptions available in the literature to obtain high-mass stars; for example, one may consider the effect of repulsive hyperon–hyperon interactions [45,46] or repulsive hyperonic three-body forces [47–49] or even a phase transition to deconfined quark matter [50,51].

In this work, we obtained two different models of neutron stars within the effective chiral model [43], namely, one which includes the octet of baryons ( $n, p, \Lambda^0, \Sigma^{-,0,+}, \Xi^{-,0}$ )

and another with delta baryons ( $n, p, \Delta^{+,+,0,-}$ ). There have been studies on the impact of the  $\Delta$  baryons of NSs within the density-dependent relativistic mean field formalism on various stellar oscillations like radial [52,53] and non-radial [54] oscillations. Our aim was to investigate the effects of hyperons and  $\Delta$  baryons on the non-radial  $f$ -mode oscillations.

This work is organized as follows. In Section 2, we give the details of the model considered. Subsequently, we describe the formulation of  $f$ -mode analysis in Section 3, which discusses the stellar structure, Cowling approximation and tidal deformability. The results obtained are discussed in Section 4. Finally, we provide a conclusion in Section 5. Throughout this paper, we choose units such that  $G = \hbar = c = 1$ , where  $G$  is the universal gravitational constant,  $\hbar$  is the reduced Planck constant and  $c$  is the speed of light.

## 2. Model

The effective Lagrangian introduced in Ref. [43] was applied here, in which the nucleon isospin doublet  $\psi_B$  interacts through the exchange of the pseudo-scalar meson  $\pi$ , the scalar meson  $\sigma$ , the iso-vector meson  $\rho$  and the vector meson  $\omega$ :

$$\begin{aligned} \mathcal{L} = & \bar{\psi}_B \left[ \left( i\gamma^\mu \partial^\mu - g_{\omega B} \gamma_\mu \omega^\mu - \frac{1}{2} g_{\rho B} \vec{\rho}_\mu \cdot \vec{\tau} \gamma^\mu \right) - g_{\sigma B} (\sigma + i\gamma_5 \vec{\tau} \cdot \vec{\pi}) \right] \psi_B \\ & + \frac{1}{2} (\partial_\mu \vec{\pi} \cdot \partial^\mu \vec{\pi} + \partial_\mu \sigma \partial^\mu \sigma) - \frac{\lambda}{4} (x^2 - x_0^2)^2 - \frac{\lambda b}{6m_B^2} (x^2 - x_0^2)^3 \\ & - \frac{\lambda c}{8m_B^4} (x^2 - x_0^2)^4 - \frac{1}{4} F_{\mu\nu} F^{\mu\nu} + \frac{1}{2} g_{\omega B}^2 x^2 (\omega_\mu \omega^\mu) \\ & - \frac{1}{4} R_{\mu\nu} \cdot R^{\mu\nu} + \frac{1}{2} m_\rho'^2 \vec{\rho}_\mu \cdot \vec{\rho}^\mu + \eta_1 \left( \frac{1}{2} g_{\rho B}^2 x^2 \vec{\rho}_\mu \cdot \vec{\rho}^\mu \right). \end{aligned}$$

Following the interaction terms of the isospin doublet  $\psi_B$ , we have the kinetic and the non-linear terms in the pion field  $\pi$  and the scalar field  $\sigma$  and the higher order terms of the scalar field in terms of  $x^2 = \pi^2 + \sigma^2$ . The last two lines include the field strength and the mass term for the fields  $\omega$  and  $\rho$ . The final term includes the effects of cross-coupling between the  $\sigma$  and  $\rho$  mesons, and the coupling strength is denoted by  $\eta_1$ . We consider only the normal non-pion condensed state of matter and hence we take  $\langle \pi \rangle = 0$  and  $m_\pi = 0$ . The scalar field attains the vacuum expectation value  $x_0$  due to the spontaneous symmetry breaking (SSB) of the chiral symmetry. The masses of the baryon ( $m_B$ ), the scalar meson ( $m_\sigma$ ) and the vector meson ( $m_\omega$ ) are then given by

$$m_B = g_{\sigma B} x_0, \quad m_\sigma = \sqrt{2\lambda} x_0, \quad m_\omega = g_{\omega B} x_0, \quad (1)$$

where  $\lambda = (m_\sigma^2 - m_\pi^2)/2f_\pi^2$ , with  $f_\pi$  being the pion decay constant which reflects the strength of the SSB. Due to the cross-coupling between the  $\sigma$  and  $\rho$  mesons, the mass of the  $\rho$  meson gets modified by the vacuum expectation value of the  $\sigma$  meson as  $m_\rho^2 = m_\rho'^2 + \eta_1 g_{\rho B}^2 x_0^2$ .

This model was earlier applied to study matter at a finite temperature and low density, and also the structure and composition of neutron stars [42,55]. The details of the model considered in this work can be found in [13], where its role in the suppression of  $r$ -mode oscillations was also studied in detail. As mentioned before, here we studied two different models, one that incorporates the octet of baryons ( $B = n^0, p^+, \Lambda^0, \Sigma^{+,0,-}, \Xi^{-,0}$ ) and another that includes delta baryons ( $n^0, p^+, \Delta^{+,+,0,-}$ ), within the same parameterization. The expressions for the energy density and the pressure of the models considered are given by

$$\begin{aligned} \epsilon = & \frac{1}{\pi^2} \sum_B \int_0^{k_{FB}} k^2 \sqrt{k^2 + m_B^{*2}} dk + \frac{m_B^2}{8C_{\sigma B}} (1 - Y^2)^2 \\ & - \frac{b}{12C_{\sigma B} C_{\omega B}} (1 - Y^2)^3 + \frac{c}{16m_B^2 C_{\sigma B} C_{\omega B}^2} (1 - Y^2)^4 \\ & + \frac{1}{2} m_\rho^2 \left[ 1 - \eta_1 (1 - Y^2) (C_{\rho B} / C_{\omega B}) \right] (\rho_{3B}^0)^2 \\ & + \frac{1}{2} m_\omega^2 \omega_0^2 Y^2 + \frac{1}{\pi^2} \sum_L \int_0^{k_{FL}} k^2 \sqrt{k^2 + m_L^2} dk, \end{aligned} \quad (2)$$

$$\begin{aligned} p = & \frac{1}{3\pi^2} \sum_B \int_0^{k_{FB}} \frac{k^4}{\sqrt{k^2 + m_B^{*2}}} dk - \frac{m_B^2}{8C_{\sigma B}} (1 - Y^2)^2 \\ & + \frac{b}{12C_{\sigma B} C_{\omega B}} (1 - Y^2)^3 - \frac{c}{16m_B^2 C_{\sigma B} C_{\omega B}^2} (1 - Y^2)^4 \\ & + \frac{1}{2} m_\rho^2 \left[ 1 - \eta_1 (1 - Y^2) (C_{\rho B} / C_{\omega B}) \right] (\rho_{3B}^0)^2 \\ & + \frac{1}{2} m_\omega^2 \omega_0^2 Y^2 + \frac{1}{3\pi^2} \sum_L \int_0^{k_{FL}} \frac{k^4}{\sqrt{k^2 + m_L^2}} dk. \end{aligned} \quad (3)$$

Here,  $k_{FB}$  is the fermi momentum of baryons, and  $Y$  is a dimensionless variable defined as  $x/x_0$ . Also,  $C_{\sigma B}$ ,  $C_{\omega B}$  and  $C_{\rho B}$ , for a given baryon,  $B$ , are the coupling constants for  $\sigma$ ,  $\omega$  and  $\rho$  respectively. The subscripts  $B$  and  $L$  denote the baryons and leptons under consideration, respectively. To obtain the EoS, the stellar matter must satisfy the conditions of charge neutrality and chemical equilibrium. The model parameters are listed in Table 1, along with their saturation properties.

**Table 1.** Parameters of the present model, such as the scalar, vector and iso-vector nucleon–meson coupling and its higher order interaction terms (top two rows), and the respective saturation properties (bottom two rows) are displayed.

$C_\sigma$ ( $fm^2$ )	$C_\omega$ ( $fm^2$ )	$C_\rho$ ( $fm^2$ )	$b$ ( $fm^2$ )	$c$ ( $fm^4$ )	$\eta_1$
8.81	2.16	13.00	12.08	−36.47	−0.85
E/A (MeV)	$(m^*/m)$	K (MeV)	$J_0$ (MeV)	$L_0$ (MeV)	$J_1$ (MeV)
−16	0.84	210	32	60	24

### 3. F-Mode Analysis

In this section, we describe the well-known Cowling approximation for non-radial oscillations along with the stellar structure equations and tidal deformability. The line element for a static, spherically symmetric relativistic NS is given as

$$ds^2 = e^{2\Phi(r)} dt^2 - e^{2\bar{\lambda}(r)} dr^2 - r^2 (d\theta^2 + \sin^2 \theta d\phi^2). \quad (4)$$

Here,  $\Phi(r)$  and  $\bar{\lambda}(r)$  are the metric functions. The solutions obtained by solving the Einstein Field equations for the given metric are the Tolman–Oppenheimer–Volkoff (TOV) equations [56,57]. They are as follows:

$$\frac{dp}{dr} = - \frac{[\epsilon + p][m + 4\pi r^3 p]}{r(r - 2m)}, \quad (5)$$

$$\frac{dm}{dr} = 4\pi r^2 \epsilon. \quad (6)$$

The TOV equations were integrated from the center to the surface of the NS to obtain the mass ( $M$ ) and radius ( $R$ ) of the star. Towards the center of the star, the value of the pressure  $p_c = p(r = 0) = p(\rho_c)$  and  $m_c = m(r = 0) = 0$ , where  $\rho_c$  is the central density. The pressure tends to zero as it approaches the surface of the star. We obtained different configurations of the global properties (like  $M$ ,  $R$  and the compactness ( $C = M/R$ )) of the NS by repeating the integration for different central densities.

Next, we proceeded to obtain the  $f$ -mode frequencies using the Cowling approximation [17], as given in Ref. [19–21], for which we made use of the solutions obtained from Equations (5) and (6) to solve the following set of coupled differential equations:

$$\frac{dW(r)}{dr} = \frac{d\epsilon}{dp} \left[ \omega^2 r^2 e^{\bar{\lambda}(r)-2\Phi(r)} V(r) + \frac{d\Phi(r)}{dr} W(r) \right] - l(l+1)e^{\bar{\lambda}(r)} V(r), \quad (7)$$

$$\frac{dV(r)}{dr} = 2 \frac{d\Phi(r)}{dr} V(r) - \frac{1}{r^2} e^{\bar{\lambda}(r)} W(r). \quad (8)$$

The functions  $V(r)$  and  $W(r)$ , along with the frequency  $\omega$ , characterize the Lagrange displacement vector ( $\eta^i$ ) associated with perturbed fluid:

$$\eta^i = \left( e^{-\bar{\lambda}(r)} W(r), -V(r) \partial_\theta, -V(r) \sin^{-2} \theta \partial_\phi \right) \frac{Y_{lm}(\theta, \phi)}{r^2},$$

where  $Y_{lm}(\theta, \phi)$  are the spherical harmonics. The differential Equations (7) and (8) obey the following boundary conditions towards the center of the star:

$$W(r) = Ar^{l+1}, \quad V(r) = -\frac{A}{l} r^l. \quad (9)$$

Here,  $A$  is an arbitrary constant, and  $l$  can take values of 2, 3, 4, etc. We did not consider  $l = 1$  because dipole oscillations do not give rise to gravitational waves [58]. The above differential equations were solved with some initial guess for  $\omega^2$ . The eigen frequency  $\omega$  should satisfy the boundary condition at the surface given below:

$$\omega^2 e^{\bar{\lambda}(R)-2\Phi(R)} V(R) + \frac{1}{R^2} \frac{d\Phi(r)}{dr} \Big|_{r=R} W(R) = 0. \quad (10)$$

Equations (7) and (8) were integrated from the center ( $r = 0$ ) to the surface ( $r = R$ ), such that the boundary condition above was met. After each integration, the initial guess of  $\omega^2$  was modified and the calculations were repeated. Here, we used Ridders's method to obtain the  $f$ -mode or eigen frequency.

The tidal deformability  $\Lambda$  depends on the EoS through both the neutron star radius  $R$  and the dimensionless Love number  $k_2$  as  $\Lambda = 2k_2 R^5/3$ . To calculate  $k_2$  for our EoS, we used the equations described in [59,60]. For a static, spherically symmetric star in a static external quadrupolar tidal field,  $\mathcal{E}_{ij}$ , the tidal deformability of a linear order is defined as  $Q_{ij} = -\Lambda \mathcal{E}_{ij}$ , where  $Q_{ij}$  is the star's induced quadrupole moment. The  $l = 2$  tidal Love number  $k_2$  in terms of  $\Lambda$  and  $R$  is given as  $k_2 = (3/2)\Lambda R^{-5}$ . To calculate  $\Lambda$ , we solved the following set of coupled first-order differential equations [60]:

$$\frac{dH}{dr} = \beta, \quad (11)$$

$$\begin{aligned} \frac{d\beta}{dr} &= 2\left(1 - 2\frac{m}{r}\right)^{-1} H \left\{ -2\pi[5\epsilon + 9p + \mathcal{A}(\epsilon + p)] \right. \\ &+ \left. \frac{3}{r^2} + 2\left(1 - 2\frac{m}{r}\right)^{-1} \left(\frac{m}{r^2} + 4\pi r p\right)^2 \right\} \\ &+ \frac{2\beta}{r} \left(1 - 2\frac{m}{r}\right)^{-1} \left\{ -1 + \frac{m}{r} + 2\pi r^2(\epsilon - p) \right\}. \end{aligned} \quad (12)$$

Here,  $\beta(r) = dH/dr$  and  $\mathcal{A} = d\epsilon/dp$ . The above equations were combined with Equations (5) and (6) and solved simultaneously. The integration is performed outwards starting at the values  $H(r) = a_0 r^2$  and  $\beta(r) = 2a_0 r$  as  $r \rightarrow 0$ . The constant  $a_0$  cancels out in the expression of the Love number and can therefore be chosen arbitrarily. It measures the deformation of the star. Since the stress–energy tensor  $T_{\mu\nu} = 0$  outside the star,  $H(r)$  is given in terms of the associated Legendre functions  $Q_2^2(r/m - 1) \sim r^{-3}$  and  $P_2^2(r/m - 1) \sim r^2$  at a large  $r$ . The interior and exterior solutions are matched at  $r = R$  to obtain a unique solution. Defining the following quantity,  $y = R\beta(R)/H(R)$ , for the solution at the interior, the  $l = 2$  Love number is given as [60]

$$\begin{aligned} k_2 &= \frac{8C^5}{5} (1 - 2C)^2 [2 + 2C(y - 1) - y] \\ &\times \left\{ 2C[6 - 3y + 3C(5y - 8)] \right. \\ &+ 4C^3[13 - 11y + C(3y - 2) + 2C^2(1 + y)] \\ &+ \left. 3(1 - 2C)^2 [2 - y + 2C(y - 1)] \ln(1 - 2C) \right\}^{-1}, \end{aligned} \quad (13)$$

where  $C = M/R$  denotes the compactness of the star. We used the prescriptions given above for the stellar structure, non-radial oscillations and tidal deformability to study the  $f$ -mode oscillations for both hyperon and  $\Delta$  baryon EoSs.

#### 4. Results and Discussions

As mentioned before, we considered charge-neutral neutron star matter populated with hyperons and another EoS with  $\Delta$  baryons, along with nucleons and leptons. In the present work, we chose a scalar coupling, and while keeping it alike for different hyperon species, we tuned the vector counterpart so as to reproduce the respective hyperon potentials and analyze the resulting effect on the EoS and the neutron star properties. The hyperon couplings were defined with respect to the nucleon, such as the scalar coupling  $x_{\sigma H} = \frac{g_{\sigma H}}{g_{\sigma N}}$ , the vector coupling  $x_{\omega H} = \frac{g_{\omega H}}{g_{\omega N}}$  and the iso-vector coupling  $x_{\rho H} = \frac{g_{\rho H}}{g_{\rho N}}$  for any hyperon species,  $H$ . The binding energy of the hyperon species in symmetric nuclear matter could then be reproduced by the equation

$$\left(\frac{B}{A}\right)_H = x_{\omega H} g_{\omega N} \omega_0 + m_H^* - m_H. \quad (14)$$

In the equation above,  $m_H^* = m_H \times Y$  is the effective mass of a particular hyperon species in matter. Recent experimental data indicate that the  $\Lambda$  and  $\Xi$  hyperons are bound with energies of  $-28$  MeV and  $-14$  MeV, respectively [61,62]. It may also be noted that a very recent study reported the potential depth of  $\Xi$  to be  $\approx -20$  MeV [63]. Therefore, in the present work, we set  $U_{\Xi} = -20$  MeV. Also, we fixed the  $\Sigma$  coupling by choosing the potential depth  $U_{\Sigma} = 30$  MeV [62]. Throughout our calculation, we fixed  $x_{\rho H} = x_{\omega H}$ .



In the absence of any experimental data on the  $\Delta$  potential, we fixed the corresponding couplings  $x_{\sigma\Delta} = x_{\rho\Delta} = x_{\omega\Delta} = 1.2$  [64], similarly to the ratio of the mass of  $\Delta$  to nucleons.

The energy density versus the pressure of the models considered here is plotted in Figure 1a. It can be seen that the softening effect of the EoS was much prominent in the case of hyperon-rich matter. This is understandable because most of the hyperons which appear in the neutron star matter happen to be lighter than the  $\Delta$  baryons and hence appear early, as well as constituting an appreciable percentage of the neutron star matter. This is in contrast to the case of the  $\Delta$  (1232) baryons, for which the only species that appeared substantially in the charge-neutral star matter was  $\Delta^-$ . This underlying difference in the EoS and the composition of the neutron star matter must be reflected in the related global properties of the neutron star, which we discuss next.

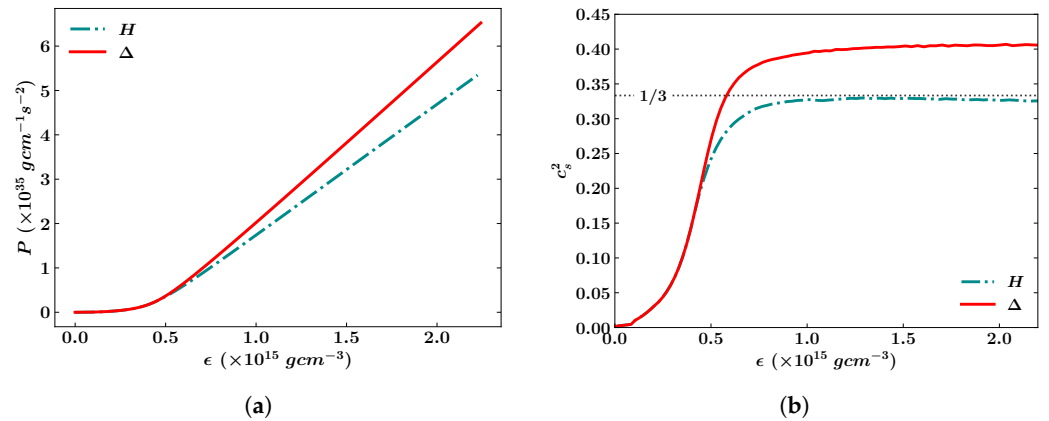


**Figure 1.** (a) Hyperonic ( $H$ ) and delta ( $\Delta$ ) equations of state of the models considered and (b) the square of the speed of sound as a function of the energy density for the EoSs. The conformal limit  $c_s^2 = 1/3$  is given by the dotted gray line.

We plotted the square of the speed of sound ( $c_s^2 = dp/d\epsilon$ ) as a function of the energy density  $\epsilon$  in Figure 1b. The speed of sound is a measure of the stiffness of stellar matter, as evident from the plot, which shows that the hyperon-rich star matter was softer than the matter with  $\Delta$  baryons. At roughly  $2\rho_0$ , where  $\rho_0$  is the normal nuclear density, the exotic particles started to appear, and therefore the softening effect on the EoS could be seen at that particular density. Causality requires the speed of sound to satisfy the constraint  $c_s^2 \leq 1$ , while it has to satisfy the condition  $c_s^2 > 0$  for thermodynamic stability. Furthermore, the perturbative quantum chromodynamics (QCD) results for extreme-density matter assume an upper limit of  $c_s^2 = 1/3$ . The EoS with  $\Delta$  baryons did not satisfy the perturbative QCD results beyond  $2\rho_0$ . Recently, several studies [65–67] have shown that the  $2M_\odot$  constraints require a speed of sound squared that is greater than the conformal limit ( $c_s^2 = 1/3$ ), indicating that the matter within the NS is a strongly interacting system. Our model with  $\Delta$  baryons resulted in a stiffer EoS. Therefore, we note that the value of  $c_s^2$  depends greatly on the internal composition of the model considered.

We plotted the mass–radius profiles obtained by numerically solving the TOV equations given by Equations (5) and (6) from the center to the surface of the star for the  $H$  and  $\Delta$  EoSs, shown in Figure 2. We obtained the maximum mass (and corresponding radius) for the  $H$  and  $\Delta$  EoSs as  $2.03M_\odot$  (12.11 km) and  $2.20M_\odot$  (12.26 km), respectively. The corresponding central densities were  $(1.89$  and  $1.84) \times 10^{15} \text{ g cm}^{-3}$ , respectively. We noted that the  $\Delta$  baryon matter resulted in a stiffer equation of state, which thereby gave a higher value for the maximum mass. In Figure 2, we have also given the observational constraints from PSR J0348+0432 ( $M = 2.01^{+0.04}_{-0.04}M_\odot$  ( $1-\sigma$  confidence interval)) [4] and the pulsar PSR J0740+6620 ( $2.14^{+0.10}_{-0.09}M_\odot$  ( $1-\sigma$  confidence interval; the  $2-\sigma$  confidence interval is  $2.14^{+0.20}_{-0.18}M_\odot$ )) [6,68]. We found that the maximum masses of the  $H$  and  $\Delta$  EoSs satisfied the

given observational constraints. Furthermore, the radius corresponding to the canonical mass  $M_{1.4}$  for both the  $H$  and  $\Delta$  EoSs was 13.38 and 13.31 km, respectively, which is in good agreement with the NICER data of the pulsar PSR J0030+0451 [69,70] and GW170817 observations [2].

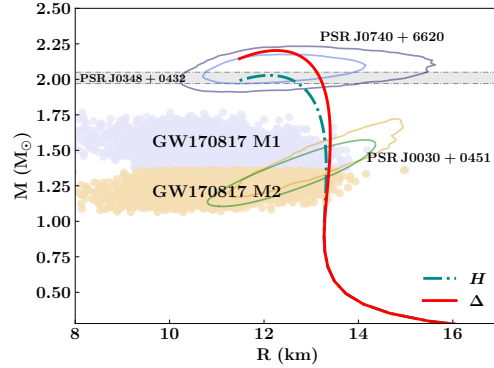


**Figure 2.** Maximum mass,  $M$ , versus radius,  $R$ , plot of the non-rotating hyperon  $H$  and  $\Delta$  baryon EoSs. The horizontal band represent the observational limit of PSR J0348+0432 ( $M = 2.01^{+0.04}_{-0.04} M_{\odot}$  [4]. Other limits from the NICER data of PSR J0740+6620 ( $2.14^{+0.20}_{-0.18} M_{\odot}$  ( $2\text{-}\sigma$  confidence interval) [6,68]) and PSR J0030+0451 [69,70] are also given. The observational constraints from the GW170817 [2] event are also shown.

Next, we proceeded to calculate the  $f$ -mode oscillation frequencies using Cowling approximation as discussed in Section 3. We solved the differential equations given by Equations (7) and (8) and repeated the integration for different values of  $\omega$  until the condition given in Equation (10) was satisfied. In Figure 3a, we show the plot of the  $f$ -mode frequencies as a function of the mass for the  $l = 2, 3$  and  $4$  modes for both the  $H$  and  $\Delta$  EoSs. We found that the  $f$ -mode frequencies of the  $H$  and  $\Delta$  EoSs showed a noticeable change in the higher mass region ( $M > 1.2M_{\odot}$ ), while the mode frequencies were similar in the lower mass region. The  $l = 2$  mode frequencies ( $f_{\max}$ ) corresponding to the maximum mass for the  $H$  and  $\Delta$  baryon EoSs were 2.42 and 2.39 kHz. We found that  $f_{\max}$  was slightly decreased for the  $\Delta$  EoS. The  $f_{\max}$  values for  $l = 3$  ( $4$ ) for the  $H$  and  $\Delta$  EoSs were 2.94 (3.42) kHz and 2.98 (3.43) kHz, respectively. It is seen from Figure 3a that the  $f$ -mode frequencies of both the EoSs increased with the mass until it attained a certain value. The  $f$ -mode frequencies for  $l = 2, 3$  and  $4$  for both  $H$  and  $\Delta$  lay approximately in the ranges of 1.84–2.42, 2.24–3 and 2.56–3.43 kHz, respectively, for a mass ranging from  $0.8M_{\odot}$  to the maximum mass profile. We found that the frequencies of the  $l = 2$  mode obtained for the  $\Delta$  EoS model lay within the range of mode frequencies obtained in Ref. [54] with different  $\Delta$  EoSs.

Next, we obtained the values of compactness,  $C = M/R$ , and surface redshift,  $Z_s = 1/\sqrt{1 - 2C} - 1$ , as a function of the  $f$ -mode frequency for the stellar models considered. The compactness of an NS quantifies how tightly its mass is packed within its radius, whereas the surface redshift measures how much light is redshifted as it escapes from the intense gravitational field of the star. The  $f$ -mode frequencies as a function of  $Z_s$  were plotted and are shown in Figure 3b. The values of compactness ( $C_{\max}$ ) and redshift ( $Z_s^{\max}$ ) corresponding to the maximum mass for the  $H$  ( $\Delta$ ) EoSs were 0.246 (0.266) and 0.403 (0.462), respectively. The  $C_{\max}$  obtained for the  $\Delta$  EoS was higher than that of the  $H$  EoS due to the stiffness of the  $\Delta$  EoS. Various observations have provided the values for redshift as  $Z_s = 0.12\text{--}0.23$  (E 1207.4-5209 [71]) and  $Z_s = 0.205^{+0.006}_{-0.003}$  (RX J0720.4-3125 [72]). We found that the values of redshift obtained for the  $H$  and  $\Delta$  EoSs satisfied these observational limits.



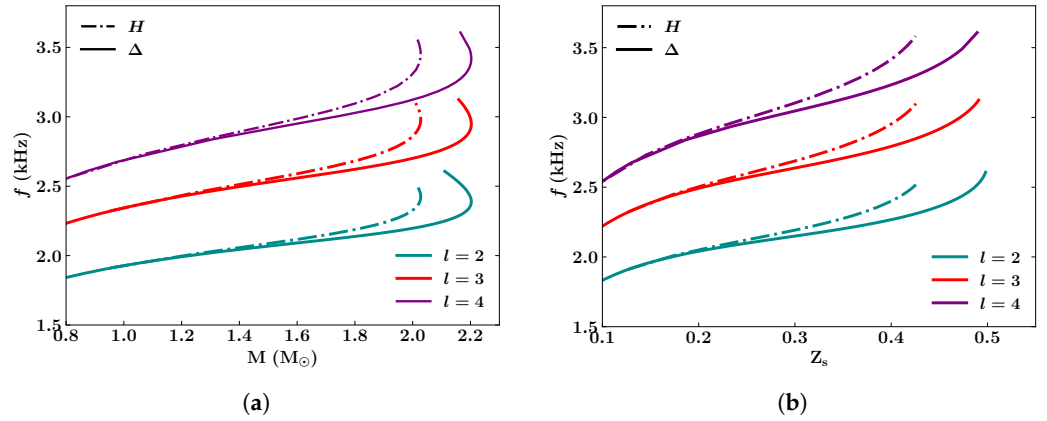


**Figure 3.**  $f$ -mode frequencies as function of NS mass  $M$  (a) and redshift  $Z_s$  (b) for  $l = 2, 3$  and  $4$  modes of oscillation.

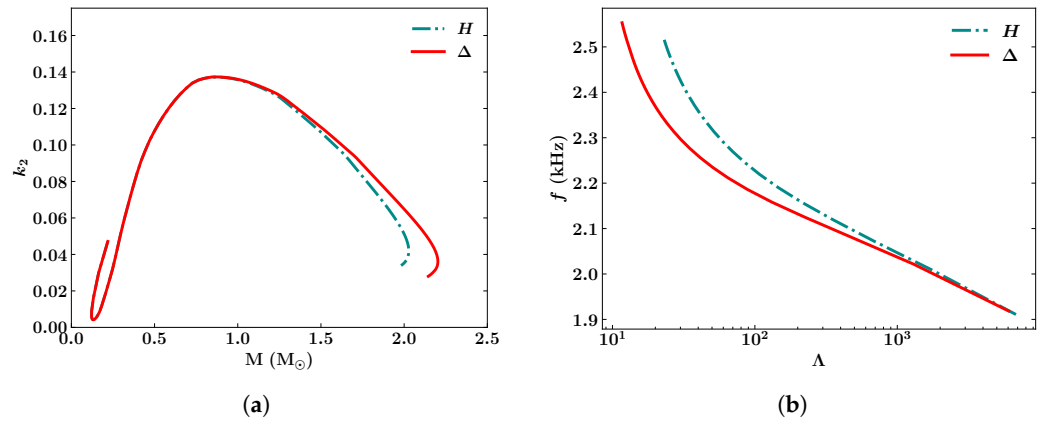


**Figure 4.** (a) The tidal Love number  $k_2$  versus the stellar mass  $M$  and (b) the  $f$ -mode frequencies,  $f$ , as a function of the tidal deformability  $\Lambda$  for the EoSs considered.

The tidal deformability provides key information about the neutron star matter. We calculated the dimensionless Love number ( $k_2$ ) using Equation (14). In Figure 4a, we display a plot of  $k_2$  versus the mass,  $M$ , of the stellar models considered. The value of  $k_2$  remained the same for both of the EoSs considered until it attained a maximum value of  $\sim 0.137$ , which had a corresponding mass value of  $\sim 0.9M_\odot$ . Then, the value of  $k_2$  decreased gradually and attained a value corresponding to the maximum mass ( $k_2^{\max}$ ) of 0.042 and 0.036 for the  $H$  and  $\Delta$  EoSs, respectively. The tidal deformability ( $\Lambda$ ) could be obtained from the Love number  $k_2$  and the stellar radius ( $R$ ) using the relation  $k_2 = 2\Lambda R^{-5}/3$ . We plotted the  $f$ -mode frequencies as a function of  $\Lambda$  for the models considered, displayed in Figure 4b. The  $f$ -mode frequencies as a function of  $\Lambda$  for the  $H$  and  $\Delta$  EoSs were easily distinguishable, and in both cases the  $\Lambda$  values decreased with an increase in the  $f$ -mode frequency until a certain value, and then they remained almost constant. The values of  $\Lambda$  corresponding to the maximum mass for the  $H$  and  $\Delta$  EoSs were 30.5 and 17.8, respectively. The event GW190814 set a limit on the canonical tidal deformability of  $\Lambda_{1.4} = 616_{-158}^{+273}$  [3]. The values of  $\Lambda_{1.4}$  for the  $H$  and  $\Delta$  EoSs were around  $\sim 800$ , which was in agreement with the constraint given by the GW event. Furthermore, in Ref. [28], the authors combined the constraints on the EoSs allowed by terrestrial nuclear experiments and tidal deformability data from GW170817. This gave them the limit for the  $f$ -mode frequency of a NS with  $1.4M_\odot$  as 1.67–2.18 kHz. We noted that the  $f$ -mode frequencies corresponding to a  $1.4M_\odot$

configuration for both the  $H$  and  $\Delta$  EoSs were approximately  $\sim 2$  kHz, which was in agreement with the given limit.

Next, we studied the  $f$ -mode oscillations by varying the potential depth  $U_\Sigma$  for  $H$  models and the coupling constants for  $\Delta$  baryons. In Figure 5, we display the plot of the  $f$ -mode frequencies for the  $l = 2$  mode as a function of the NS mass for different parameterizations:  $U_\Sigma = -10$  MeV and  $+30$  MeV, and  $x_{\sigma\Delta} = x_{\rho\Delta} = x_{\omega\Delta} = 0.8, 1.0, 1.2$ . We noted that the maximum mass increased when  $U_\Sigma$  was decreased from  $+30$  to  $-10$  MeV. However, we found that the maximum mass showed only a negligible change when we varied the coupling constants of  $\Delta$  baryons. We found that the range of  $f$ -mode frequencies did not change when varying the values of the  $\Sigma$  potential and delta coupling constants. The  $f$ -mode frequencies corresponding to the maximum mass ( $f_{\max}$ ) did not change considerably when either the  $\Sigma$  potentials or coupling constants were varied.

The fundamental idea behind gravitational wave asteroseismology is the same as that in traditional helioseismology, where stellar oscillations are studied to infer the properties of the interior of a star. Here, we proceeded to obtain a linear fit of the  $f$ -mode frequencies as a function of the average density, which was given as  $f$  (kHz)  $\approx a + b\sqrt{\tilde{M}/\tilde{R}^3}$  (here,  $\tilde{M} = M/1.4M_\odot$  and  $\tilde{R} = R/10$  km) for our EoSs. In Ref. [73], the authors calculated the fitting relation using a polytropic EoS for the first time as  $f$  (kHz)  $\approx 0.17 + 2.3\sqrt{\tilde{M}/\tilde{R}^3}$ . This relation was later modified by the authors for relativistic EoSs [74] to  $f$  (kHz)  $\approx 0.78 + 1.635\sqrt{\tilde{M}/\tilde{R}^3}$ . Furthermore, in Ref. [75], the authors obtained empirical relations using hybrid EoSs. Recently, empirical relations using hyperonic and dark matter EoSs have been obtained in [23] and [25], respectively.

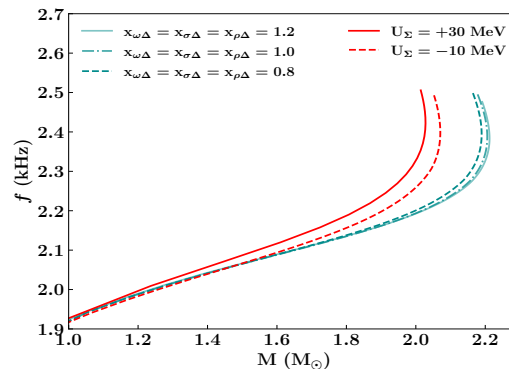


**Figure 5.** The  $l = 2$   $f$ -mode frequencies as a function of the NS mass  $M$  for different EoSs obtained by varying the coupling constants and the potential depth of  $\Sigma$  within the effective chiral model.

We plotted the  $f$ -mode frequencies as a function of the average density for different parameterizations of the  $H$  and  $\Delta$  baryon models, shown in Figure 6. We also calculated a linear fit between the frequency and average density for the models considered, which was obtained as  $1.148$  kHz  $+ 1.358\sqrt{\tilde{M}/\tilde{R}^3}$  kHz. We compare the values of coefficients  $a$  and  $b$  obtained from different analyses in Table 2, and the fitting relations obtained are plotted in Figure 6. The empirical relations obtained in each case were different from one another, which was due to the difference in the composition of the matter considered inside the NS. We found that our data were closer to the fit obtained in Ref. [23]. The fitting relations can be used in order to constrain the EoS by measuring the  $f$ -mode frequency, which can be used to infer the mass and radius values.

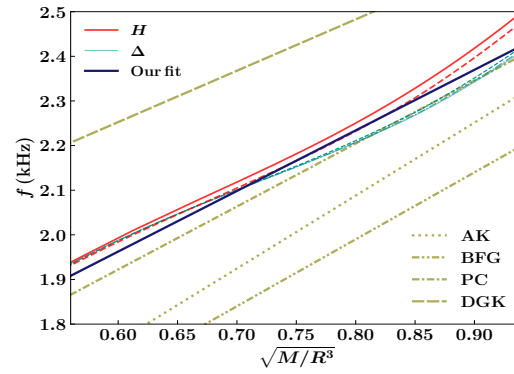


**Figure 6.**  $f$ -mode frequency as a function of the average density for the EoSs considered, indicated by the same legend as in Figure 5. The empirical relation obtained for our EoSs is given by the dark blue solid line. Other empirical relations taken from different works (N. Andersson & K. D. Kokkotas (1998) (AK) [73], O. Benhar et al. (2004) (BFG) [75], D. Doneva et al. (2013) (DGK) [11] and B. K. Pradhan & D. Chatterjee (2021) (PC) [23]) are given in an olive color.

**Table 2.** Coefficients  $a$  and  $b$  of the fitting relation,  $f$  (kHz)  $\approx a + b\sqrt{\tilde{M}/\tilde{R}^3}$ , obtained from different works, for the  $l = 2$  mode.

Works	a (kHz)	b (kHz)
N. Andersson and K. D. Kokkotas (1998) [73]	0.780	1.635
O. Benhar et al. (2004) [75]	0.790	1.500
D. Doneva et al. (2013) [11]	1.562	1.151
B. K. Pradhan and D. Chatterjee (2021) [23]	1.075	1.412
Our work	1.148	1.358

## 5. Conclusions

In this work, we studied  $f$ -mode oscillations by employing Cowling approximation in neutron stars (NSs) with hyperons ( $H$ ) and  $\Delta$  baryons, using the effective chiral model with mesonic cross-coupling within the relativistic mean field theory. We found that the square of the speed of sound violated the conformal limit ( $c_s^2 = 1/3$ ) for the  $\Delta$  EoS, indicating a strongly interacting system. The hyperonic system, on the other hand, gave a value of  $c_s^2$ , which was lower but closer to the conformal limit. We then obtained the static stellar properties of the models considered. We found that the maximum masses obtained for both the  $H$  and  $\Delta$  EoSs were consistent with the observational data of PSR J0348+0432, PSR J0740+6620 and GW170817. Then, we calculated the  $f$ -mode frequencies by employing Cowling approximation, which neglects the metric perturbations as a result of fluid oscillations. We calculated the  $f$ -mode frequency as a function of the stellar mass ( $M$ ) and redshift ( $Z_s$ ) for both the  $H$  and  $\Delta$  EoSs. We obtained the mode frequencies for masses ranging from  $0.8M_\odot$  to the maximum mass configuration in the ranges of 1.84–2.42, 2.24–3 and 2.56–3.43 kHz for  $l = 2, 3$  and 4 modes, respectively. We found that the  $f$ -mode frequency ( $f_{\max}$ ) corresponding to the maximum mass was relatively higher for the stars with the  $\Delta$  model. This was due to the greater stiffness of the  $\Delta$  EoS compared to the hyperon EoS. The results obtained from our analysis were found to agree with the observational data from different pulsars and GW events.

We also studied the tidal properties of the models considered and it was found that the values of tidal deformability ( $\Lambda$ ) for both the  $H$  and  $\Delta$  EoSs were in close agreement with the observational constraints obtained from the GW190814 event. We also obtained the  $f$ -mode frequencies as a function of  $\Lambda$ , and it was found that the mode frequency of a  $1.4M_\odot$  star was approximately  $\sim 2$  kHz for both the  $H$  and  $\Delta$  NSs. We found that our results

were in agreement with the limit provided in Ref. [28]. We hope that future observations from binary neutron star mergers could possibly provide more insights about the  $f$ -mode oscillations of NSs.

Next, we calculated the  $f$ -mode frequencies for the  $l = 2$  mode by varying the coupling constants and potential depth ( $U_{\Sigma}$ ) for  $\Delta$  baryons and hyperons, respectively. Our results show that the coupling constant had a negligible effect on both the frequencies and the mass of the stellar configuration. We also found that the ranges of the  $f$ -mode frequencies were almost the same for the models considered in our work. Further, we obtained an empirical relation (a relation obtained between the  $f$ -mode frequency and average density) for the set of EoSs considered. We also compared the relations obtained in other works with our work. We found that the empirical relations depend greatly on the internal composition of the stars.

**Author Contributions:** Conceptualization, V.S. and T.K.J.; methodology, O.P.J. and P.E.S.K.; validation, O.P.J., P.E.S.K. and V.S.; formal analysis, O.P.J. and P.E.S.K.; investigation, O.P.J., P.E.S.K., V.S., H.C. and T.K.J.; resources, O.P.J., P.E.S.K., V.S., H.C. and T.K.J.; data curation, O.P.J., P.E.S.K. and H.C.; writing—original draft preparation, O.P.J. and P.E.S.K.; writing—review and editing, V.S. and T.K.J.; visualization, V.S. and T.K.J.; supervision, V.S. and T.K.J.; funding acquisition, V.S. All authors have read and agreed to the published version of the manuscript.

**Funding:** A contribution towards the APC was given by the Provost Office, Amrita Vishwa Vidyapeetham.

**Data Availability Statement:** Data is contained within the article.

**Acknowledgments:** P.E.S.K. acknowledges the support of the Bonn-Cologne Graduate School of Physics and Astronomy (BCGS).

**Conflicts of Interest:** The authors declares no conflict of interest.

## References

- Abbott, B.P.; Abbott, R.; Abbott, T.; Acernese, F.; Ackley, K.; Adams, C.; Adams, T.; Addesso, P.; Adhikari, R.X.; Adya, V.B.; et al. GW170817: Observation of Gravitational Waves from a Binary Neutron Star Inspiral. *Phys. Rev. Lett.* **2017**, *119*, 161101. <https://doi.org/10.1103/PhysRevLett.119.161101>.
- Abbott, B.P.; Abbott, R.; Abbott, T.D.; Acernese, F.; Ackley, K.; Adams, C.; Adams, T.; Addesso, P.; Adhikari, R.X.; Adya, V.B.; et al. GW170817: Measurements of neutron star radii and equation of state. *Phys. Rev. Lett.* **2018**, *121*, 161101. <https://doi.org/10.1103/PhysRevLett.121.161101>.
- Abbott, R.; Abbott, T.D.; Abraham, S.; Acernese, F.; Ackley, K.; Adams, C.; Adhikari, R.X.; Adya, V.B.; Affeldt, C.; Agathos, M.; et al. GW190814: Gravitational Waves from the Coalescence of a 23 Solar Mass Black Hole with a 2.6 Solar Mass Compact Object. *Astrophys. J.* **2020**, *896*, L44. <https://doi.org/10.3847/2041-8213/ab960f>.
- Antoniadis, J.; Freire, P.C.; Wex, N.; Tauris, T.M.; Lynch, R.S.; Van Kerkwijk, M.H.; Kramer, M.; Bassa, C.; Dhillon, V.S.; Driebe, T.; et al. A Massive Pulsar in a Compact Relativistic Binary. *Science* **2013**, *340*, 6131. <https://doi.org/10.1126/science.1233232>.
- Fonseca, E.; Pennucci, T.T.; Ellis, J.A.; Stairs, I.H.; Nice, D.J.; Ransom, S.M.; Demorest, P.B.; Arzoumanian, Z.; Crowter, K.; Dolch, T.; et al. The NANOGrav Nine-year Data Set: Mass and Geometric Measurements of Binary Millisecond Pulsars. *Astrophys. J.* **2016**, *832*, 167. <https://doi.org/10.3847/0004-637X/832/2/167>.
- Cromartie, H.T.; Fonseca, E.; Ransom, S.M.; Demorest, P.B.; Arzoumanian, Z.; Blumer, H.; Brook, P.R.; DeCesar, M.E.; Dolch, T.; Ellis, J.A.; et al. Relativistic Shapiro delay measurements of an extremely massive millisecond pulsar. *Nat. Astron.* **2019**, *4*, 72–76. <https://doi.org/10.1038/s41550-019-0880-2>.
- Chandrasekhar, S. Solutions of Two Problems in the Theory of Gravitational Radiation. *Phys. Rev. Lett.* **1970**, *24*, 611–615. <https://doi.org/10.1103/PhysRevLett.24.611>.
- Friedman, J.L.; Schutz, B.F. Secular instability of rotating Newtonian stars. *Astrophys. J.* **1978**, *222*, 281–296. <https://doi.org/10.1086/156143>.
- Nayyar, M.; Owen, B.J. R-modes of accreting hyperon stars as persistent sources of gravitational waves. *Phys. Rev. D* **2006**, *73*, 084001. <https://doi.org/10.1103/PhysRevD.73.084001>.
- Passamonti, A.; Glampedakis, K. Nonlinear viscous damping and gravitational wave detectability of the  $f$ -mode instability in neutron stars. *Mon. Not. Roy. Astron. Soc.* **2012**, *422*, 3327. <https://doi.org/10.1111/j.1365-2966.2012.20849.x>.

11. Doneva, D.D.; Gaertig, E.; Kokkotas, K.D.; Krüger, C. Gravitational wave asteroseismology of fast rotating neutron stars with realistic equations of state. *Phys. Rev. D* **2013**, *88*, 044052. <https://doi.org/10.1103/PhysRevD.88.044052>.
12. Gittins, F.; Andersson, N. The r-modes of slowly rotating, stratified neutron stars. *Mon. Not. Roy. Astron. Soc.* **2023**, *521*, 3043–3057. <https://doi.org/10.1093/mnras/stad672>.
13. Jyothilakshmi, O.P.; Krishnan, P.E.S.; Thakur, P.; Sreekanth, V.; Jha, T.K. Hyperon bulk viscosity and r-modes of neutron stars. *Mon. Not. Roy. Astron. Soc.* **2022**, *516*, 3381–3388. <https://doi.org/10.1093/mnras/stac2360>.
14. Laskos-Patkos, P.; Moustakidis, C.C. Signatures of quark deconfinement through the r-modes of twin stars. *Phys. Rev. D* **2023**, *107*, 123023. <https://doi.org/10.1103/PhysRevD.107.123023>.
15. Passamonti, A.; Gaertig, E.; Kokkotas, K.D. The evolution of the f-mode instability and gravitational wave detection perspectives. *J. Phys. Conf. Ser.* **2013**, *453*, 012011. <https://doi.org/10.1088/1742-6596/453/1/012011>.
16. Lindblom, L.; Detweiler, S.L. The quadrupole oscillations of neutron stars. *Astrophys. J. Suppl.* **1983**, *53*, 73–92. <https://doi.org/10.1086/190884>.
17. Cowling, T.G. The Non-radial Oscillations of Polytypic Stars. *Mon. Not. Roy. Astron. Soc.* **1941**, *101*, 367–375. <https://doi.org/10.1093/mnras/101.8.367>.
18. Sotani, H.; Takiwaki, T. Accuracy of relativistic Cowling approximation in protoneutron star asteroseismology. *Phys. Rev. D* **2020**, *102*, 063025. <https://doi.org/10.1103/PhysRevD.102.063025>.
19. Sotani, H.; Yasutake, N.; Maruyama, T.; Tatsumi, T. Signatures of hadron-quark mixed phase in gravitational waves. *Phys. Rev. D* **2011**, *83*, 024014. <https://doi.org/10.1103/PhysRevD.83.024014>.
20. Flores, C.V.; Lugones, G. Discriminating hadronic and quark stars through gravitational waves of fluid pulsation modes. *Class. Quant. Grav.* **2014**, *31*, 155002. <https://doi.org/10.1088/0264-9381/31/15/155002>.
21. Ranea-Sandoval, I.F.; Guilera, O.M.; Mariani, M.; Orsaria, M.G. Oscillation modes of hybrid stars within the relativistic Cowling approximation. *J. Cosmol. Astropart. Phys.* **2018**, *12*, 031. <https://doi.org/10.1088/1475-7516/2018/12/031>.
22. Vásquez Flores, C.; Parisi, A.; Chen, C.S.; Lugones, G. Fundamental oscillation modes of self-interacting bosonic dark stars. *J. Cosmol. Astropart. Phys.* **2019**, *6*, 051. <https://doi.org/10.1088/1475-7516/2019/06/051>.
23. Pradhan, B.K.; Chatterjee, D. Effect of hyperons on f-mode oscillations in Neutron Stars. *Phys. Rev. C* **2021**, *103*, 035810. <https://doi.org/10.1103/PhysRevC.103.035810>.
24. Kumar, D.; Mishra, H.; Malik, T. Non-radial oscillation modes in hybrid stars: Consequences of a mixed phase. *J. Cosmol. Astropart. Phys.* **2023**, *2*, 015. <https://doi.org/10.1088/1475-7516/2023/02/015>.
25. Das, H.C.; Kumar, A.; Biswal, S.K.; Patra, S.K. Impacts of dark matter on the f-mode oscillation of hyperon star. *Phys. Rev. D* **2021**, *104*, 123006. <https://doi.org/10.1103/PhysRevD.104.123006>.
26. Jyothilakshmi, O.P.; Naik, L.J.; Sreekanth, V. Non-radial oscillations in anisotropic dark energy stars. *Eur. Phys. J. C* **2024**, *84*, 427. <https://doi.org/10.1140/epjc/s10052-024-12776-9>.
27. Lattimer, J.M.; Prakash, M. Neutron Star Observations: Prognosis for Equation of State Constraints. *Phys. Rept.* **2007**, *442*, 109–165. <https://doi.org/10.1016/j.physrep.2007.02.003>.
28. Wen, D.H.; Li, B.A.; Chen, H.Y.; Zhang, N.B. GW170817 implications on the frequency and damping time of f-mode oscillations of neutron stars. *Phys. Rev. C* **2019**, *99*, 045806. <https://doi.org/10.1103/PhysRevC.99.045806>.
29. Gell-Mann, M.; Levy, M. The axial vector current in beta decay. *Nuovo Cim.* **1960**, *16*, 705. <https://doi.org/10.1007/BF02859738>.
30. Lee, T.D.; Wick, G.C. Vacuum Stability and Vacuum Excitation in a Spin 0 Field Theory. *Phys. Rev. D* **1974**, *9*, 2291–2316. <https://doi.org/10.1103/PhysRevD.9.2291>.
31. Lee, T.D.; Margulies, M. Interaction of a Dense Fermion Medium with a Scalar Meson Field. *Phys. Rev. D* **1975**, *11*, 1591. <https://doi.org/10.1103/PhysRevD.12.4008>.
32. Furnstahl, R.J.; Serot, B.D. Finite nuclei in a relativistic model with broken chiral and scale invariance. *Phys. Lett. B* **1993**, *316*, 12–16. [https://doi.org/10.1016/0370-2693\(93\)90649-3](https://doi.org/10.1016/0370-2693(93)90649-3).
33. Serot, B.D. Covariant effective field theory for bulk properties of nuclei. *Ser. Adv. Quant. Many Body Theor.* **2002**, *6*, 207–216. <https://doi.org/10.1142/S0217979203020284>.
34. Heide, E.K.; Rudaz, S.; Ellis, P.J. An Effective Lagrangian with broken scale and chiral symmetry applied to nuclear matter and finite nuclei. *Nucl. Phys. A* **1994**, *571*, 713–732. [https://doi.org/10.1016/0375-9474\(94\)90717-X](https://doi.org/10.1016/0375-9474(94)90717-X).
35. Mishustin, I.; Bondorf, J.; Rho, M. Chiral symmetry, scale invariance and properties of nuclear matter. *Nucl. Phys. A* **1993**, *555*, 215–224. [https://doi.org/10.1016/0375-9474\(93\)90319-5](https://doi.org/10.1016/0375-9474(93)90319-5).
36. Papazoglou, P.; Zschesche, D.; Schramm, S.; Schaffner-Bielich, J.; Stoecker, H.; Greiner, W. Nuclei in a chiral SU(3) model. *Phys. Rev. C* **1999**, *59*, 411–427. <https://doi.org/10.1103/PhysRevC.59.411>.
37. Schramm, S. Deformed nuclei in a chiral model. *Phys. Rev. C* **2002**, *66*, 064310. <https://doi.org/10.1103/PhysRevC.66.064310>.
38. Tsubakihara, K.; Ohnishi, A. A Chiral symmetric relativistic mean field model with logarithmic sigma potential. *Prog. Theor. Phys.* **2007**, *117*, 903–921. <https://doi.org/10.1143/PTP.117.903>.



39. Tsubakihara, K.; Maekawa, H.; Matsumiya, H.; Ohnishi, A. Lambda hypernuclei and neutron star matter in a chiral SU(3) relativistic mean field model with a logarithmic potential. *Phys. Rev. C* **2010**, *81*, 065206. <https://doi.org/10.1103/PhysRevC.81.065206>.
40. Boguta, J. Abnormal nuclei. *Phys. Lett. B* **1983**, *128*, 19–23. [https://doi.org/10.1016/0370-2693\(83\)90065-5](https://doi.org/10.1016/0370-2693(83)90065-5).
41. Sahu, P.K.; Basu, R.; Datta, B. High density matter in the chiral sigma model. *Astrophys. J.* **1993**, *416*, 267–275. <https://doi.org/10.1086/173233>.
42. Jha, T.K.; Mishra, H. Constraints on nuclear matter parameters of an Effective Chiral Model. *Phys. Rev.* **2008**, *C78*, 065802. <https://doi.org/10.1103/PhysRevC.78.065802>.
43. Malik, T.; Banerjee, K.; Jha, T.K.; Agrawal, B.K. Nuclear symmetry energy with mesonic cross-couplings in the effective chiral model. *Phys. Rev.* **2017**, *C96*, 035803. <https://doi.org/10.1103/PhysRevC.96.035803>.
44. Patra, N.K.; Malik, T.; Sen, D.; Jha, T.K.; Mishra, H. An Equation of State for Magnetized Neutron Star Matter and Tidal Deformation in Neutron Star Mergers. *Astrophys. J.* **2020**, *900*, 49. <https://doi.org/10.3847/1538-4357/aba8fc>.
45. Bednarek, I.; Haensel, P.; Zdunik, J.; Bejger, M.; Manka, R. Hyperons in neutron-star cores and two-solar-mass pulsar. *Astron. Astrophys.* **2012**, *543*, A157. <https://doi.org/10.1051/0004-6361/201118560>.
46. Oertel, M.; Providência, C.; Gulminelli, F.; Raduta, A.R. Hyperons in neutron star matter within relativistic mean-field models. *J. Phys. G* **2015**, *42*, 075202. <https://doi.org/10.1088/0954-3899/42/7/075202>.
47. Vidana, I.; Polls, A.; Ramos, A.; Hjorth-Jensen, M.; Stoks, V.G.J. Strange nuclear matter within Bruckner-Hartree-Fock theory. *Phys. Rev.* **2000**, *C61*, 025802. <https://doi.org/10.1103/PhysRevC.61.025802>.
48. Yamamoto, Y.; Furumoto, T.; Yasutake, N.; Rijken, T.A. Hyperon mixing and universal many-body repulsion in neutron stars. *Phys. Rev.* **2014**, *C90*, 045805. <https://doi.org/10.1103/PhysRevC.90.045805>.
49. Lonardonì, D.; Gandolfi, S.; Pederiva, F. Effects of the two-body and three-body hyperon-nucleon interactions in  $\Lambda$ -hypernuclei. *Phys. Rev.* **2013**, *C87*, 041303. <https://doi.org/10.1103/PhysRevC.87.041303>.
50. Wei, W.; Irving, B.; Salinas, M.; Klähn, T.; Jaikumar, P. Camouflage of the Phase Transition to Quark Matter in Neutron Stars. *Astrophys. J.* **2019**, *887*, 151. <https://doi.org/10.3847/1538-4357/ab53ea>.
51. Klähn, T.; Łastowiecki, R.; Blaschke, D. Implications of the measurement of pulsars with two solar masses for quark matter in compact stars and heavy-ion collisions: A Nambu–Jona-Lasinio model case study. *Phys. Rev. D* **2013**, *88*, 085001. <https://doi.org/10.1103/PhysRevD.88.085001>.
52. Rather, I.A.; Marquez, K.D.; Panotopoulos, G.; Lopes, I. Radial oscillations in neutron stars with delta baryons. *Phys. Rev. D* **2023**, *107*, 123022. <https://doi.org/10.1103/PhysRevD.107.123022>.
53. Rather, I.A.; Marquez, K.D.; Backes, B.C.; Panotopoulos, G.; Lopes, I. Radial oscillations of hybrid stars and neutron stars including delta baryons: The effect of a slow quark phase transition. *J. Cosmol. Astropart. Phys.* **2024**, *5*, 130. <https://doi.org/10.1088/1475-7516/2024/05/130>.
54. Kalita, P.J.; Routaray, P.; Ghosh, S.; Kumar, B.; Agrawal, B.K. Probing the impact of delta-baryons on nuclear matter and non-radial oscillations in neutron stars. *J. Cosmol. Astropart. Phys.* **2024**, *4*, 065. <https://doi.org/10.1088/1475-7516/2024/04/065>.
55. Jha, T.K.; Mishra, H.; Sreekanth, V. On attributes of a Rotating Neutron star with a Hyperon core. *Phys. Rev.* **2008**, *C77*, 045801. <https://doi.org/10.1103/PhysRevC.77.045801>.
56. Tolman, R.C. Static Solutions of Einstein's Field Equations for Spheres of Fluid. *Phys. Rev.* **1939**, *55*, 364–373. <https://doi.org/10.1103/PhysRev.55.364>.
57. Oppenheimer, J.R.; Volkoff, G.M. On Massive Neutron Cores. *Phys. Rev.* **1939**, *55*, 374–381. <https://doi.org/10.1103/PhysRev.55.374>.
58. Chandrasekhar, S.; Ferrari, V. On the non-radial oscillations of a star. III—A reconsideration of the axial modes. *Proc. R. Soc. Lond. Ser. A* **1991**, *434*, 449–457. <https://doi.org/10.1098/rspa.1991.0104>.
59. Hinderer, T. Tidal Love Numbers of Neutron Stars. *Astrophys. J.* **2008**, *677*, 1216. <https://doi.org/10.1086/533487>.
60. Hinderer, T.; Lackey, B.D.; Lang, R.N.; Read, J.S. Tidal deformability of neutron stars with realistic equations of state and their gravitational wave signatures in binary inspiral. *Phys. Rev. D* **2010**, *81*, 123016. <https://doi.org/10.1103/PhysRevD.81.123016>.
61. Gomes, R.O.; Dexheimer, V.; Schramm, S.; Vasconcellos, C.A.Z. Many-body forces in the equation of state of hyperonic matter. *Astrophys. J.* **2015**, *808*, 8. <https://doi.org/10.1088/0004-637x/808/1/8>.
62. Schaffner-Bielich, J.; Gal, A. Properties of strange hadronic matter in bulk and in finite systems. *Phys. Rev. C* **2000**, *62*, 034311. <https://doi.org/10.1103/PhysRevC.62.034311>.
63. Friedman, E.; Gal, A. Constraints on  $\Xi^-$  nuclear interactions from capture events in emulsion. *Phys. Lett. B* **2021**, *820*, 136555. <https://doi.org/10.1016/j.physletb.2021.136555>.
64. Raduta, A.R.  $\Delta$ -admixed neutron stars: Spinodal instabilities and dUrca processes. *Phys. Lett. B* **2021**, *814*, 136070. <https://doi.org/10.1016/j.physletb.2021.136070>.
65. Bedaque, P.; Steiner, A.W. Sound velocity bound and neutron stars. *Phys. Rev. Lett.* **2015**, *114*, 031103. <https://doi.org/10.1103/PhysRevLett.114.031103>.



66. Moustakidis, C.C.; Gaitanos, T.; Margaritis, C.; Lalazissis, G.A. Bounds on the speed of sound in dense matter, and neutron star structure. *Phys. Rev. C* **2017**, *95*, 045801. <https://doi.org/10.1103/PhysRevC.95.045801>.
67. Tews, I.; Lattimer, J.M.; Ohnishi, A.; Kolomeitsev, E.E. Symmetry Parameter Constraints from a Lower Bound on Neutron-matter Energy. *Astrophys. J.* **2017**, *848*, 105. <https://doi.org/10.3847/1538-4357/aa8db9>.
68. Riley, T.E.; Watts, A.L.; Ray, P.S.; Bogdanov, S.; Guillot, S.; Morsink, S.M.; Bilous, A.V.; Arzoumanian, Z.; Choudhury, D.; Deneva, J.S.; et al. A NICER View of the Massive Pulsar PSR J0740+6620 Informed by Radio Timing and XMM-Newton Spectroscopy. *Astrophys. J. Lett.* **2021**, *918*, L27. <https://doi.org/10.3847/2041-8213/ac0a81>.
69. Riley, T.E.; Watts, A.L.; Bogdanov, S.; Ray, P.S.; Ludlam, R.M.; Guillot, S.; Arzoumanian, Z.; Baker, C.L.; Bilous, A.V.; Chakrabarty, D.; et al. A NICER View of PSR J0030+0451: Millisecond Pulsar Parameter Estimation. *Astrophys. J. Lett.* **2019**, *887*, L21. <https://doi.org/10.3847/2041-8213/ab481c>.
70. Miller, M.C.; Lamb, F.K.; Dittmann, A.J.; Bogdanov, S.; Arzoumanian, Z.; Gendreau, K.C.; Guillot, S.; Harding, A.K.; Ho, W.C.G.; Lattimer, J.M.; et al. PSR J0030+0451 Mass and Radius from NICER Data and Implications for the Properties of Neutron Star Matter. *Astrophys. J. Lett.* **2019**, *887*, L24. <https://doi.org/10.3847/2041-8213/ab50c5>.
71. Sanwal, D.; Pavlov, G.G.; Zavlin, V.E.; Teter, M.A. Discovery of Absorption Features in the X-Ray Spectrum of an Isolated Neutron Star. *Astrophys. J.* **2002**, *574*, L61. <https://doi.org/10.1086/342368>.
72. Hambaryan, V.; Suleimanov, V.; Haberl, F.; Schwöpe, A.D.; Neuhäuser, R.; Hohle, M.; Werner, K. The compactness of the isolated neutron star RX J0720.4–3125. *Astron. Astrophys.* **2017**, *601*, A108. <https://doi.org/10.1051/0004-6361/201630368>. <https://doi.org/10.3847/2041-8213/ab960f>.
73. Andersson, N.; Kokkotas, K.D. Gravitational Waves and Pulsating Stars: What Can We Learn from Future Observations? *Phys. Rev. Lett.* **1996**, *77*, 4134–4137. <https://doi.org/10.1103/PhysRevLett.77.4134>.
74. Andersson, N.; Kokkotas, K.D. Towards gravitational wave asteroseismology. *Mon. Not. Roy. Astron. Soc.* **1998**, *299*, 1059–1068. <https://doi.org/10.1046/j.1365-8711.1998.01840.x>.
75. Benhar, O.; Ferrari, V.; Gualtieri, L. Gravitational wave asteroseismology revisited. *Phys. Rev. D* **2004**, *70*, 124015. <https://doi.org/10.1103/PhysRevD.70.124015>.

**Disclaimer/Publisher’s Note:** The statements, opinions and data contained in all publications are solely those of the individual author(s) and contributor(s) and not of MDPI and/or the editor(s). MDPI and/or the editor(s) disclaim responsibility for any injury to people or property resulting from any ideas, methods, instructions or products referred to in the content.